nature photonics

ARTICLES

PUBLISHED ONLINE: 15 JUNE 2015 | DOI: 10.1038/NPHOTON.2015.105

Macroscopic and direct light propulsion of bulk graphene material

Tengfei Zhang[1†], Huicong Chang[1†], Yingpeng Wu[1†], Peishuang Xiao[1], Ningbo Yi[1], Yanhong Lu[1], Yanfeng Ma[1], Yi Huang[1], Kai Zhao[1], Xiao-Qing Yan[2], Zhi-Bo Liu[2], Jian-Guo Tian[2] and Yongsheng Chen[1*]

It has been a great challenge to achieve the direct light manipulation of matter on a bulk scale. In this work the direct light propulsion of matter is observed on a macroscopic scale using a bulk graphene-based material. The unique structure and properties of graphene, and the novel morphology of the bulk three-dimensional linked graphene material make it capable not only of absorbing light at various wavelengths but also of emitting energetic electrons efficiently enough to drive the bulk material, following Newtonian mechanics. Thus, the unique photonic and electronic properties of individual graphene sheets are manifested in the response of the bulk state. These results offer an exciting opportunity to bring about bulk-scale light manipulation with the potential to realize long-sought applications in areas such as the solar sail and space transportation driven directly by sunlight.

Using beams of light, scientists have been able to trap[1], move[2], levitate[3] and even pull[4] small objects (such as atoms and molecules, living cells and viruses, and micro/nanoscopic particles) on the microscopic scale, as well as nano/micrometre-sized graphene sheets[5–7] on a small spatial scale, typically on the order of hundreds of micrometres[8]. There have also been reports of efforts to enlarge the optical manipulation distance by harnessing strong thermal forces[9], and also the robust manipulation of airborne micro-objects photophoretically with a bottle beam[10]. Furthermore, the rotation and motion of a millimetre-sized graphite disk by photoirradiation has been realized with the graphite levitated magnetically[11]. If these optical operations were to be achieved with large objects on a macroscopic spatial scale, significant applications such as the long-sought direct optical manipulation of macroscale objects (including the proposed solar sail and space transportation via laser or beam-powered propulsion) could be realized. To acquire the required energy and momentum for propulsion, two main mechanisms have been proposed: the use of a laser to superheat a propellant (or air), which then provides propulsion in the same manner as a conventional rocket[4,12,13], or obtaining propulsion directly from light pressure (radiation pressure) acting on a light sail structure (as with the IKAROS spacecraft)[14,15].

It has been a great challenge to realize the intrinsic properties of single-layer graphene in the bulk state, because stacking of the graphene sheets diminishes most of its properties (electronic, photonic and even mechanical). In this Article, we show that if graphene sheets are assembled in the proper manner into the bulk state, the resulting bulk material not only can retain the intrinsic properties of the individual graphene sheets, but also allows their manifestation on a macroscopic scale. Here, we demonstrate the directly light-induced macroscopic propulsion and rotation of a bulk graphene sponge material with dimensions on the scale of a centimetre and milligram weight. The mechanism behind this novel phenomenon is believed to be an efficient light-induced ejected electron emission process that follows an Auger-like path due both to the unique band structure of graphene and the macroscopic morphology of this unique material. The force generated from such a process/mechanism is much larger than the force generated directly from conventional light pressure (which is much smaller than the force required to propel the samples). A series of control experiments were also carried out that excluded the laser beam ablation mechanism. The efficient light absorption of graphene[16,17] and easily achievable reverse saturation state[18,19], combined with the unique and limited hot-electron relaxing mechanisms and channels[17,20] (all due to the unique band structure of graphene), collectively make this bulk graphene material capable of efficiently emitting energetic electrons while under light illumination, such that the net momentum generated by the ejected electrons can propel the bulk graphene sponge according to Newton's laws of motion.

The graphene sponge was synthesized using a modified version of a previously reported method[21], followed by a high-temperature annealing step in an inert environment. Details of the procedure are provided in Supplementary Section 'Materials synthesis', as well as additional optical images of bulk material of different sizes (Supplementary Fig. 1). The material has a conductivity of $\sim 0.5\ S\ m^{-1}$ and a density of $\sim 1\ mg\ ml^{-1}$.

When cutting the graphene sponge by laser in air, we serendipitously observed this laser-induced actuation with the naked eye, and it contrasted sharply with the previously reported microscopic levitation or movement of micro objects due to light pressure[3,8]. To avoid the probable interference of air, further systematic studies were carried out entirely in vacuum (from 6.8×10^{-4} to 5×10^{-6} torr) to rule out (minimize) the possibility of heated air disturbances and to avoid local combustion of the graphene sponge due to the presence of oxygen. The experimental set-up is shown in Fig. 1 for both direct light-induced propulsion (Fig. 1a) and rotation (Fig. 1b) of our bulk graphene samples. To rule out any effects from friction, electrostatic attraction or collision between the sample and the tube during

[1]Key Laboratory of Functional Polymer Materials and Center for Nanoscale Science and Technology, Collaborative Innovation Center of Chemical Science and Engineering, Institute of Polymer Chemistry, College of Chemistry, Nankai University, Tianjin 300071, China. [2]Key Laboratory of Weak Light Nonlinear Photonics, Ministry of Education, Teda Applied Physics School and School of Physics, Nankai University, Tianjin 300457, China. †These authors contributed equally to this work. *e-mail: yschen99@nankai.edu.cn

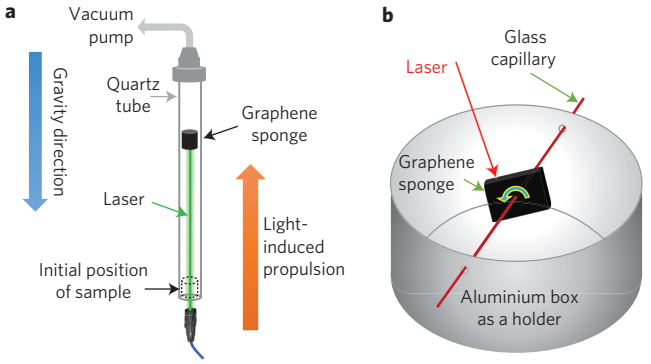

Figure 1 | Measurement apparatus and schematics of light-induced propulsion and rotation of graphene sponge. a, Schematic of the graphene sponge being propelled vertical upwardly with laser illumination from below. **b**, Apparatus for light-induced rotation of graphene sponge under laser illumination.

light-induced propulsion, an investigation of light-induced rotation was performed with the apparatus in Fig. 1b to discover any quantitative relationship or mechanism. For this, the graphene sponge was cut into a cuboid and a glass capillary (or metal wire) acted as an axis penetrating through the centre of the sample.

Light-induced horizontal and vertical propulsion

First, as shown in Supplementary Movie 1, macroscopic graphene objects (with centimetre-scale size) could be pushed away immediately when the laser beam was applied, and lasers with different wavelengths (450, 532 and 650 nm) produced the same phenomenon. More surprisingly, when the graphene objects were placed at the bottom of a vertical vacuum tube, direct and instant optical vertical upward propulsion to sub-metre height (limited by the vacuum facilities) was observed (Fig. 2a,b and Supplementary Movie 2) when the laser beam was directed under the sample. Figure 2a demonstrates that, when lasers with the same power density but different wavelengths were used, at the same moment after illumination of the same sample, higher propulsion heights were observed with lasers with shorter wavelengths (Supplementary Movie 2). As shown in Fig. 2b (Supplementary Fig. 2), the propulsion height increased with increasing laser power density if the laser wavelength was fixed, no matter what laser wavelength was used. A similar dependence was also observed when the sample was placed in a horizontal vacuum tube (not shown). Given the above results and the well-known band structure of graphene (which in principle allows the absorption of all wavelengths of light[16,17]), we used simulated sunlight generated by a xenon lamp as the light source for the same set-up. Strikingly similar direct sunlight-induced horizontal and vertical propulsions were achieved (Supplementary Movie 3). Furthermore, by varying the distance between the light source and the sample to obtain light of different intensities, the vertical propulsion height varied accordingly (Supplementary Fig. 3). Significantly, on using natural sunlight on a sunny day with a Fresnel lens for focusing, a similar optical response was observed (Supplementary Movie 4).

Rotation with different light wavelengths and intensities

As mentioned above, the propulsion heights and speeds change with light intensity and wavelength for a given sample, but, to avoid other factors such as friction, electrostatic attraction and also collision between the sample and the tube during the light-induced propulsion, the home-made device shown in Fig. 1b was used to obtain a quantitative relationship for laser-induced rotation (Supplementary Movie 5) with different light wavelengths and power densities. Figure 2c presents a summary of the results for rotation speed versus laser power density/wavelength. Because the rotational kinetic energy E is proportional to the square of the rotation speed r and sample mass $m(E \propto mr^2)$, the square of rotation speed was plotted against the laser wavelength and laser power density (for a detailed discussion see Supplementary Section 'Rotation speed and rotational kinetic energy'). Indeed, as shown in Fig. 2d, we found that, for the same sample, the square of rotation speed (rotational kinetic energy) increased linearly with increasing laser power density at a constant wavelength for all laser beam tests (450, 532, 650 nm), and this dependence holds independently of the size and mass of the samples (Fig. 2e and Supplementary Fig. 4). Similarly, at a given laser power density, lasers with shorter wavelengths (higher frequency and photon energy) gave a larger value for the square of the rotation speed (Fig. 2d), following the similar linear relationship demonstrated more clearly in Fig. 2f.

Mechanism of macroscopic and direct light propulsion

Before investigating and discussing the possible mechanism for this surprising bulk-scale and direct light manipulation, the composition (Supplementary Table 1 and Figs 5–7), morphology and structure (Supplementary Figs 8–10) of the graphene sponge were investigated thoroughly. Based on these results and reports from elsewhere[21–23], the graphene sponge should be a three-dimensional crosslinked monolithic graphene material, where the graphene sheets, as the building unit, are covalently crosslinked together through reactions between the oxygenic functional groups located mostly on the sheets edges during the solvothermal process. In other words, this material can be thought of as a three-dimensional crosslinked but graphene-based polymer, where graphene sheets of different size act as the monomers. The C–O covalent bonds located mainly at the graphene sheet edges not only structurally hold the whole material as a bulk and monolithic object, but also act as an electronic barrier and electronically induce quantum confinement between the graphene sheets through a localized bandgap[24–26]. Therefore, each of the graphene sheets or sp^2 domains in the bulk material can be considered as an electronically isolated and structurally suspended individual graphene sheet. Overall, the graphene sponge can be seen and treated electronically as a sum of many individual graphene sheets, but without exhibiting the strong coupling properties of the graphene sheets (as is the case for graphite). Thus, the Dirac-type band structure should essentially be maintained for the individual graphene sheets in the graphene sponge, but with a slightly opened bandgap, which should allow the material to behave as a collection of individual suspended graphene sheets while retaining the intrinsic properties of graphene[17,27,28]. Note that the photon energy of the lasers we used is at least ~1.91 eV, which should be much higher than the opened but possibly very small bandgap[29,30] of the individual graphene sheets in the graphene sponge.

Two working mechanisms have been well-documented for beam-powered propulsion[13]: an external laser beam ablates/burns off propellant to provide a propulsion that is similar to conventional chemical rockets[12,13], or the direct radiation pressure generates a propulsion force governed by Maxwell's electromagnetism theory, as has been proposed for the solar sail[14,15]. The light intensities (irradiance) of the watt-level laser and simulated sunlight in our tests were at 10^5 and 10^4 W m^{-2} levels, respectively. Based on radiation pressure theory, the propulsion forces produced by the radiation pressure of such a laser and simulated sunlight should both be ~10^{-9} N and are orders of magnitude smaller than the force required to move and propel the bulk graphene object (for details see Supplementary Section 'Calculation of radiation pressure'). So, the direct radiation pressure-induced mechanism can be excluded. Another possibility for explaining our laser-induced propulsion and rotation is the conventional laser beam ablating or burning off of graphene material to generate a plasma plume or carbon particles and molecules for propulsion. However, such a mechanism

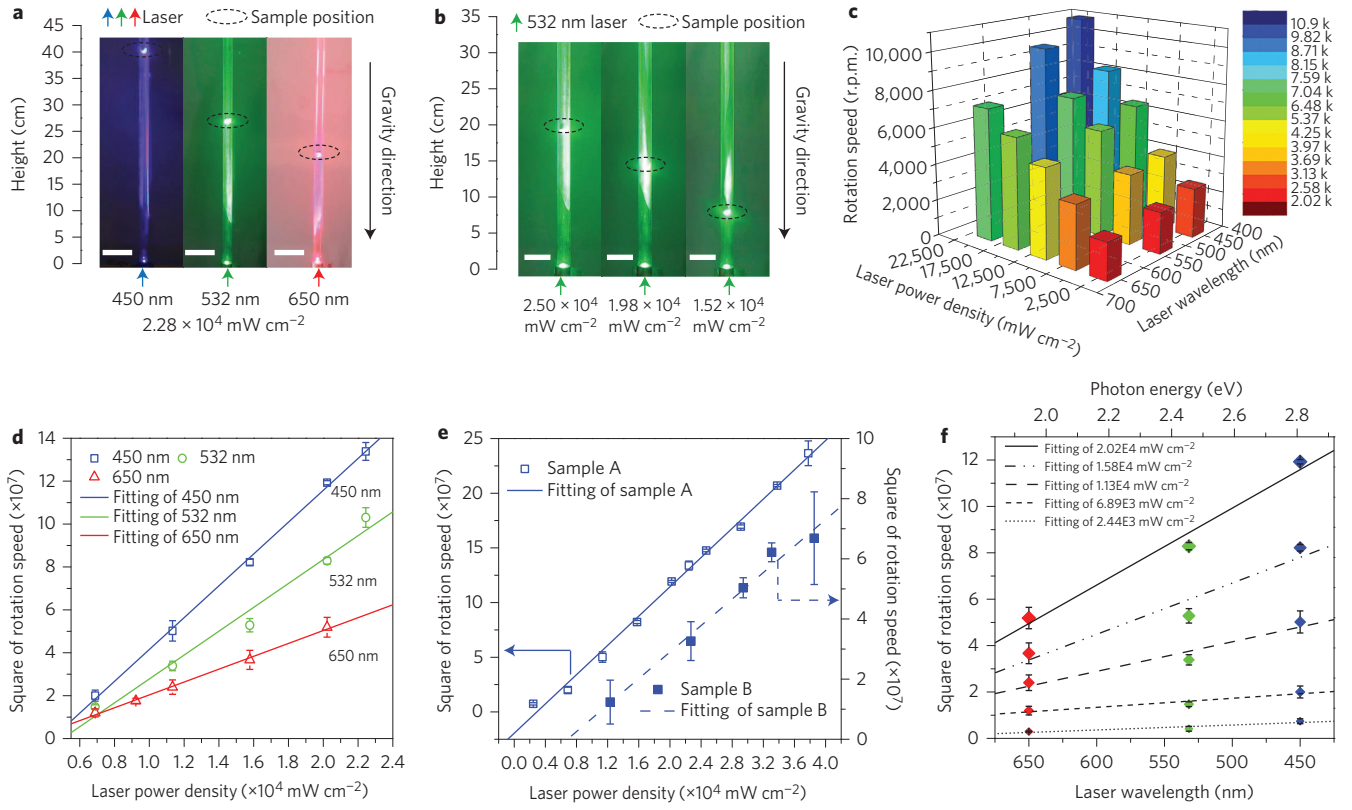

Figure 2 | Relationships between laser-induced propulsion/rotation of graphene sponge and laser wavelength and power density. a, Different vertical propulsion heights of the same sample over the same time (2 s) and with the same power density but different wavelengths (scale bars, 5 cm). **b**, Different vertical propulsion heights of the same sample over the same time (1 s) and with the same wavelength but different power densities (scale bars, 5 cm). **c**, Three-dimensional histogram showing the rotation speed of the graphene sponge sample, showing a distinct positive correlation with power density and frequency of the laser. **d**, The square of rotation speed increases linearly with laser power density, and lasers with different wavelengths give similar results. **e**, Linear relationship of laser power density and square of rotation speed for different samples (laser wavelength, 450 nm). **f**, For a given sample, the square of rotation speed increases almost linearly with a decrease in laser wavelength (or increase in photon energy) under the same laser power density (450, 532 and 650 nm, blue, green and red diamonds; the bigger the diamond, the higher the laser power density.) Error bars in **d**–**f** are the variance S^2 of rotation speed.

usually needs an extremely high-power laser supply, so pulsed laser sources (micro/nanosecond-level pulse width and gigawatt-level peak power) or ultrahigh-power continuous-wave lasers (up to megawatt level) have been used[13]. This contrasts with our light-induced motion, which can be observed even with sunlight, which has a much lower power. Note that the continuous-wave lasers used here were only at the watt level. Furthermore, all the experimental results we have discussed so far exclude such a mechanism. First, after repeated testing on all the graphene sponge samples, no noticeable ablation or combustion trace was observed, and there was no evidence of weight reduction (for details see Supplementary Section 'No weight reduction of graphene sponge under laser illumination'). Second, no detectable carbon clusters or other small molecular pieces/particles from the graphene sponge were observed under our watt-level continuous-wave laser illumination, even using high-resolution mass spectrometers in the mass/charge range of 12–4,000 (Supplementary Figs 11 and 12). Finally, it should be noted that graphene and graphite can withstand high temperatures without decomposing[31], and the fabrication of our material involves annealing at 800 °C in the last step. Based on these observations, we believe that direct laser ablation is unlikely to provide the main driving force in our experiments.

These results prompted us to search for other possible mechanisms for macroscopic direct light manipulation. It is well known that graphene sheet has unique optoelectronic properties due to its Dirac conical and gapless band structure, which allows graphene (1) to absorb all wavelengths of light efficiently, (2) to easily achieve a population inversion state as a result of the excitation of hot electrons and the bottleneck of the relaxation at the Dirac point, and then (3) to eject hot electrons following a proposed Auger-like mechanism[16–19,32–34]. Many studies of this effect have been reported, not only for individual suspended graphene sheets[17,18], but also for reduced graphene oxide sheets[29]. In the competition among the different relaxation pathways of carriers in the reverse saturated state of optically excited graphene, due to weak electron–phonon coupling, the Auger-like recombination proves to be the dominant process and plays an unusually strong role in the relaxation dynamics process[20,34–36] of the hot carriers (electrons). It has also been reported that fully suspended graphene has a much greater photoresponsivity than graphene on a support[17,37]. As discussed above, our bulk graphene material could be treated as a macroscopic collection of many electronically isolated and suspended individual graphene sheets, so a bulk-scale sum of such a photoresponse should be observed due to the macroscopic addition of many individual and suspended graphene sheets in this unique graphene material. So, with continuous laser/light excitation, long-lived photoexcited and energetic hot carriers (electrons) would be excited into the conduction band, and a population inversion could be generated and maintained. Note that such a distribution of hot carriers could be obtained in two ways: by increasing the absorbed photon density (laser power density) or by increasing the photon energy (laser frequency). These are completely

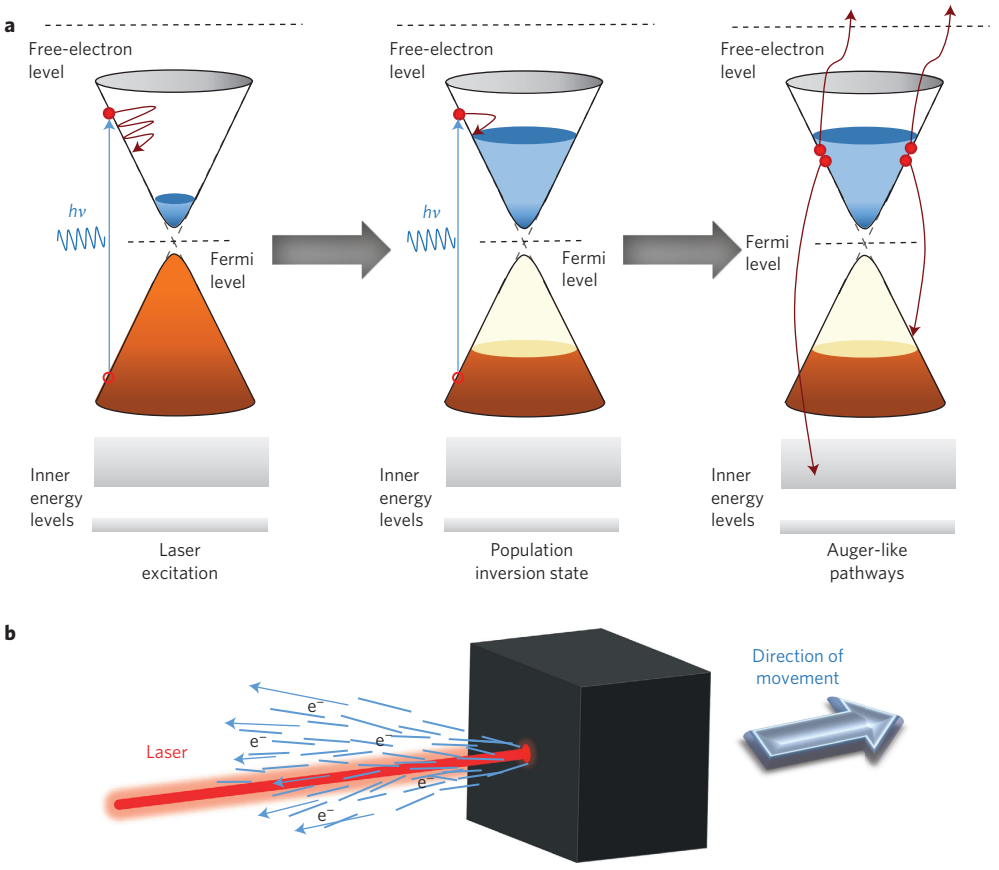

Figure 3 | Schematic diagrams of the proposed mechanism. a, Schematic of the proposed mechanism of electron emission. The laser excites electrons from the valence band to the conduction band, and a population inversion state is achieved and maintained. Some hot electrons obtain enough energy to be ejected and become free electrons through Auger-like pathways. **b**, Schematic diagram showing the net emitted electrons flying away from the graphene sponge and propelling the graphene object along the laser propagation direction.

interchangeable[38] and also supported by our results. We thus argue that Auger-like recombination is probably the dominant path for the relaxation of hot electrons for our photoexcited graphene and, if it involves the inner energy levels as in the classical Auger effect, will result in hot carriers (electrons) being ejected out as free electrons once they obtain enough energy (Fig. 3a)[34,36,38]. Note that the ejected electrons will be emitted randomly in all directions; some will be absorbed by the surrounding graphene sponge, some will generate a mutually offsetting force, and only the net electrons ejected in the direction opposite the laser beam propagation direction can contribute to the net propulsion and push the sample in the direction of the beam (Fig. 3b).

Measurement of ejected electrons

To verify the mechanism we designed a device to collect the ejected electrons from the graphene sponge under laser illumination (Fig. 4a). The sample was placed inside a metal box (as the electron-collecting electrode), which was positioned in a vacuum chamber with a quartz window for laser illumination. On illuminating the graphene sponge with a 450 nm, 1.5 W chopped continuous-wave laser, a strong cycling current signal appeared immediately. This matched the chopped laser beam cycling (Fig. 4b). Similar results were also observed using lasers with other wavelengths (Supplementary Fig. 13). More results for the current signal intensity obtained with different wavelengths and power densities are shown in Fig. 4c (also Supplementary Figs 13 and 14), where the average current due to the electron ejection rate is seen to have a linear relationship with the laser power density for the same laser wavelength, as well as a linear relationship with laser wavelength (or photon energy) for the same laser power density. The energy of the emitted electrons was further measured using a home-modified X-ray photoelectron spectroscope (XPS). The results are shown in Fig. 4d, where a broad kinetic energy distribution is observed for the ejected electrons. We also measured a series of control materials, including carbon nanotubes, with the same device under the same conditions, but negligible current signals were obtained (Supplementary Fig. 15).

It is possible that the electron emission is due to the conventional thermionic mechanism (Edison effect) following the Richardson equation ($J = A_G T^2 \exp(-w/kT)$, where J is the emission current density, A_G is the Richardson constant, T is the temperature of the metal, w is the work function of the metal, and k is the Boltzmann constant), which depends exponentially on temperature[39]. If this is the case, temperature effects should be observed—the heating/cooling process is much slower than the rather fast photonic process. However, in the plot of *in situ* (real-time) time versus current shown in Fig. 4e and Supplementary Fig. 16, neither the current intensity nor the pattern show such a time-related effect for any tests with different laser pulse widths in a wide range from 1,000 ms to 2 ms. Furthermore, our estimates show that the temperature of the graphene sponge could not be higher than 900 °C under our laser pulse illumination, even assuming all the laser energy was converted to heat (for details see Supplementary Section 'The possible highest temperature of the graphene sponge sample under illumination of laser pulse') without any energy loss. Note that the efficient thermionic emission temperature is usually at least 1,000 °C for most materials[40] and even higher for carbon nanotubes and graphene[41,42]. Finally, as shown

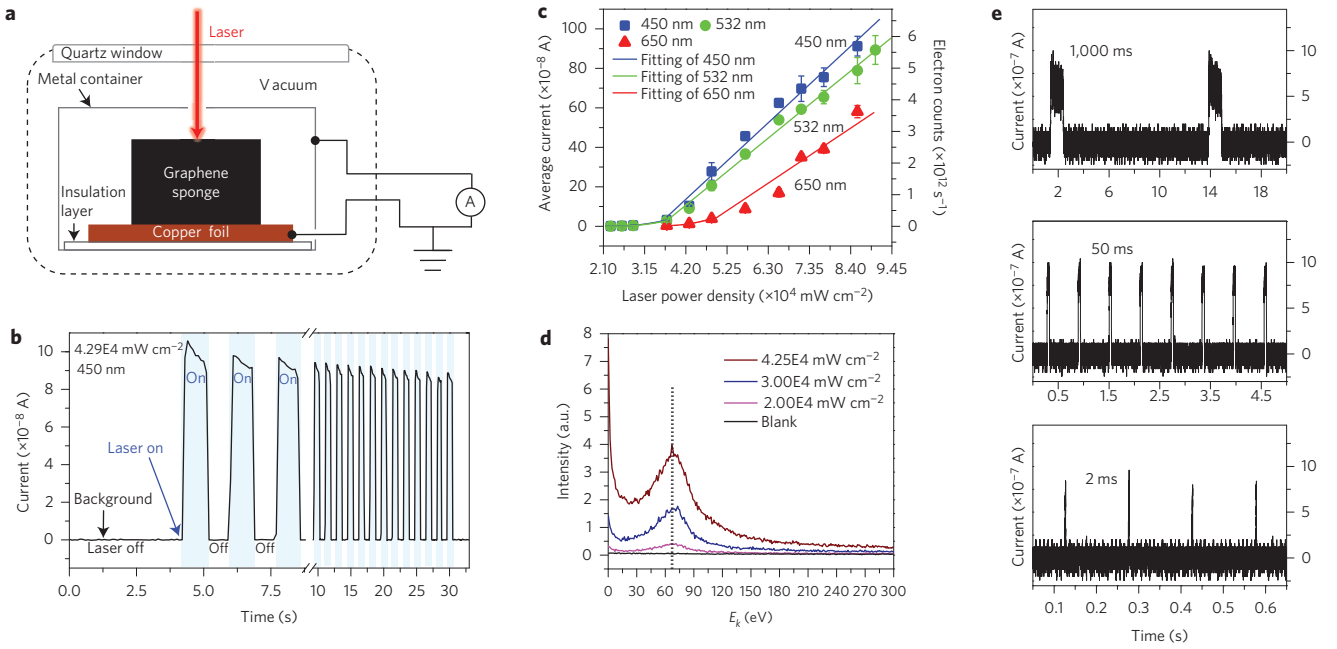

Figure 4 | Measurement of electron emission from the graphene sponge under laser illumination. a, Schematic of the device for measuring electrons emitted from the sample. **b**, A typical curve obtained by measuring the current intensity, with the on–off state of the laser controlled by a chopper. **c**, The average current signal intensity could be obtained (for details see Supplementary Section 'Mathematical calculation of the average current signal intensity') and, for a given laser wavelength, the intensity increased linearly with laser power density over a wide range. Error bars represent standard deviation (s.d.) for the same repeated measurements. **d**, Kinetic energy distribution spectrum of electrons emitted from graphene sponge under laser (450 nm) illumination, showing a broad energy distribution. **e**, Current signals under laser pulse illumination with different pulse widths (1,000, 50 and 2 ms). Neither a time-related delay impact nor meaningful current intensity change can be observed. The slight difference between signals is probably a result of measurement error.

in Fig. 4c and Supplementary Fig. 14, under the same laser power density the current signal intensity has a clear wavelength dependence. In combination with the well-known fact that graphene has efficient absorption over the full spectrum (Supplementary Fig. 17), the above results indicate that the thermionic mechanism, at least, should not be the major path[41]. So, above all, the electron emission of the graphene sponge under laser illumination should essentially be a direct photo-induced process.

With all these experimental results, the remaining question is whether the kinetic energy generated by the ejected electrons is large enough to move/propel the sample. The average current was measured at $\sim 3.0 \times 10^{-8}$–9.0×10^{-7} A under a laser power of 1.3–3.0 W (450 nm, power density of 3.71×10^{4}–8.57×10^{4} mW cm^{-2} for a 3.5 mm^2 laser spot, Fig. 4c), which means that the electron ejection rate should be $\sim 2.0 \times 10^{11}$–5.7×10^{12} s^{-1}, so a power of 2.2×10^{-6}–6.4×10^{-5} J s^{-1} (W) could be obtained based on an average kinetic energy (Fig. 4d) of 70 eV for the ejected electrons. This is larger than the energy necessary (<10^{-6} W) to vertically propel the sample (for details see Supplementary Section 'Estimation of the energy conversion in the laser-induced propulsion and rotation'). Rotation is easier to achieve than laser-induced vertical propulsion. Note that the actual propulsion force/energy should be significantly larger than the values estimated above, as clearly not all the electrons were collected in the measurement. Thus, this propulsion by light-induced ejected electrons (LIEE) is in fact an energy transfer process, where the photon energy is absorbed by graphene bulk materials and converted into the kinetic energy of ejected electrons, rather than a direct momentum transfer process as in the previously proposed propulsion by light pressure. In light of the rather complicated relaxation process for light-induced hot electrons at the reverse saturated state, which involves several continuous steps and competing paths, many more works, including a comprehensive theoretical modelling and some ultrafast dynamic measurements, are needed to fully understand this novel phenomenon and verify our hypothesis for the mechanism.

Discussion

It is important to emphasize that the remarkable light-induced macroscale propulsion reported herein is a result of the unique electronic band structure at the Dirac point and the associated optoelectronic properties of the graphene sheet itself, together with the unique macro structural character of this novel bulk graphene material. Obviously, other two-dimensional materials with a similar Dirac conical band structure (such as graphynes[43], silicene[44], planar Ge[45] and two-dimensional $Bi_{1-x}Sb_x$ thin films[46]), if assembled in a similar way, might show similar LIEE phenomena when illuminated with light. Accordingly, some macroscopic practical utilization of the optical force, only observed for microscale light actuation to date[2,8], may be achieved based on this work. Furthermore, in this process, propulsion is generated by the ejected electrons, which is completely different from conventional laser ablation propulsion. Although the propulsion energy/force is still small compared with conventional chemical rockets, it is already several orders of magnitude larger than that from light pressure. Assuming that the area of a typical solar-cell panel structure on a satellite is ~50 m^2 and, because a laser–graphene sponge-based rocket does not need other moving parts, with a payload of 500 kg the acceleration rate would be 0.09 m s^{-2}. Because the density of graphene sponge is very low and no other onboard propellant is needed (the required vacuum and light are naturally available in space), the theoretical specific impulse of our laser propulsion could be much higher. Furthermore, the material could also be used as a novel and convenient electron emission source.

In summary, our results demonstrate that macro graphene-based objects could be propelled directly by a watt-level laser, and even sunlight, up to the sub-metre scale, following a novel LIEE mechanism. The propulsion could be further enhanced by increasing the

light intensity and/or improving the illumination area. For example, using an adjustable laser array, the force needed for attitude control and orbital adjustment of a spacecraft, and even transporting a payload in outer space, could be achieved using light directly. As well as graphene, other two-dimensional materials with a Dirac conical band structure are also expected to demonstrate this striking property. These results also suggest that exotic and unprecedented properties or phenomena could be obtained when these unique two-dimensional materials are assembled in such a way that their intrinsic two-dimensional properties are retained.

Methods

Methods and any associated references are available in the online version of the paper.

Received 2 March 2015; accepted 19 May 2015; published online 15 June 2015

References

1. Ashkin, A. Acceleration and trapping of particles by radiation pressure. *Phys. Rev. Lett.* **24,** 156–159 (1970).
2. Grier, D. G. A revolution in optical manipulation. *Nature* **424,** 810–816 (2003).
3. Swartzlander, G. A., Peterson, T. J., Artusio-Glimpse, A. B. & Raisanen, A. D. Stable optical lift. *Nature Photon.* **5,** 48–51 (2011).
4. Dogariu, A., Sukhov, S. & Saenz, J. J. Optically induced 'negative forces'. *Nature Photon.* **7,** 24–27 (2013).
5. Kane, B. Levitated spinning graphene flakes in an electric quadrupole ion trap. *Phys. Rev. B* **82,** 115441 (2010).
6. Marago, O. M. *et al.* Brownian motion of graphene. *ACS Nano* **4,** 7515–7523 (2010).
7. Twombly, C. W., Evans, J. S. & Smalyukh, I. I. Optical manipulation of self-aligned graphene flakes in liquid crystals. *Opt. Express* **21,** 1324–1334 (2013).
8. Ashkin, A. History of optical trapping and manipulation of small-neutral particle, atoms, and molecules. *IEEE J. Sel. Top. Quantum Electron.* **6,** 841–856 (2000).
9. Shvedov, V. G. *et al.* Giant optical manipulation. *Phys. Rev. Lett.* **105,** 118103 (2010).
10. Shvedov, V. G., Hnatovsky, C., Rode, A. V. & Krolikowski, W. Robust trapping and manipulation of airborne particles with a bottle beam. *Opt. Express* **19,** 17350–17356 (2011).
11. Kobayashi, M. & Abe, J. Optical motion control of maglev graphite. *J. Am. Chem. Soc.* **134,** 20593–20596 (2012).
12. Ageev, V. P. *et al.* Experimental and theoretical modeling of laser propulsion. *Acta Astronaut.* **7,** 79–90 (1980).
13. Phipps, C. *et al.* Review: laser-ablation propulsion. *J. Propul. Power* **26,** 609–637 (2010).
14. Tsu, T. C. Interplanetary travel by solar sail. *ARS J.* **29,** 422–427 (1959).
15. Tsuda, Y. *et al.* Flight status of IKAROS deep space solar sail demonstrator. *Acta Astronaut.* **69,** 833–840 (2011).
16. Nair, R. R. *et al.* Fine structure constant defines visual transparency of graphene. *Science* **320,** 1308 (2008).
17. Patil, V., Capone, A., Strauf, S. & Yang, E. H. Improved photoresponse with enhanced photoelectric contribution in fully suspended graphene photodetectors. *Sci. Rep.* **3,** 2791 (2013).
18. Li, T. *et al.* Femtosecond population inversion and stimulated emission of dense Dirac fermions in graphene. *Phys. Rev. Lett.* **108,** 167401 (2012).
19. Perakis, I. E. Stimulated near-infrared light emission in graphene. *Physics* **5,** 43 (2012).
20. Strait, J. H. *et al.* Very slow cooling dynamics of photoexcited carriers in graphene observed by optical-pump terahertz-probe spectroscopy. *Nano Lett.* **11,** 4902–4906 (2011).
21. Wu, Y. *et al.* Three-dimensionally bonded spongy graphene material with super compressive elasticity and near-zero Poisson's ratio. *Nature Commun.* **6,** 6141 (2015).
22. Xu, Y., Sheng, K., Li, C. & Shi, G. Self-assembled graphene hydrogel via a one-step hydrothermal process. *ACS Nano* **4,** 4324–4330 (2010).
23. Zhou, Y., Bao, Q., Tang, L. A. L., Zhong, Y. & Loh, K. P. Hydrothermal dehydration for the 'green' reduction of exfoliated graphene oxide to graphene and demonstration of tunable optical limiting properties. *Chem. Mater.* **21,** 2950–2956 (2009).
24. Wehling, T. O., Katsnelson, M. I. & Lichtenstein, A. I. Impurities on graphene: midgap states and migration barriers. *Phys. Rev. B* **80,** 085428 (2009).
25. Wu, X. *et al.* Epitaxial-graphene/graphene-oxide junction: an essential step towards epitaxial graphene electronics. *Phys. Rev. Lett.* **101,** 026801 (2008).
26. Loh, K. P., Bao, Q. L., Eda, G. & Chhowalla, M. Graphene oxide as a chemically tunable platform for optical applications. *Nature Chem.* **2,** 1015–1024 (2010).
27. Meyer, J. C. *et al.* The structure of suspended graphene sheets. *Nature* **446,** 60–63 (2007).
28. Prechtel, L. *et al.* Time-resolved ultrafast photocurrents and terahertz generation in freely suspended graphene. *Nature Commun.* **3,** 646 (2012).
29. Kim, J. *et al.* Unconventional terahertz carrier relaxation in graphene oxide: observation of enhanced Auger recombination due to defect saturation. *ACS Nano* **8,** 2486–2494 (2014).
30. Eda, G., Mattevi, C., Yamaguchi, H., Kim, H. & Chhowalla, M. Insulator to semimetal transition in graphene oxide. *J. Phys. Chem. C* **113,** 15768–15771 (2009).
31. Campos-Delgado, J. *et al.* Thermal stability studies of CVD-grown graphene nanoribbons: defect annealing and loop formation. *Chem. Phys. Lett.* **469,** 177–182 (2009).
32. Winzer, T., Knorr, A. & Malic, E. Carrier multiplication in graphene. *Nano Lett.* **10,** 4839–4843 (2010).
33. Winzer, T. & Malic, E. Impact of Auger processes on carrier dynamics in graphene. *Phys. Rev. B* **85,** 241404 (2012).
34. Winzer, T., Malic, E. & Knorr, A. Microscopic mechanism for transient population inversion and optical gain in graphene. *Phys. Rev. B* **87,** 165413 (2013).
35. Brida, D. *et al.* Ultrafast collinear scattering and carrier multiplication in graphene. *Nature Commun.* **4,** 1987 (2013).
36. Gabor, N. M. Impact excitation and electron–hole multiplication in graphene and carbon nanotubes. *Acc. Chem. Res.* **46,** 1348–1357 (2013).
37. Gabor, N. M. *et al.* Hot carrier-assisted intrinsic photoresponse in graphene. *Science* **334,** 648–652 (2011).
38. Tielrooij, K. J. *et al.* Photoexcitation cascade and multiple hot-carrier generation in graphene. *Nature Phys.* **9,** 248–252 (2013).
39. Dushman, S. Electron emission from metals as a function of temperature. *Phys. Rev.* **21,** 623–636 (1923).
40. Turner, L. W. (ed) *Electronics Engineer's Reference Book* 4th edn (Newnes-Butterworth, 1976).
41. Yaghoobi, P., Moghaddam, M. V. & Nojeh, A. 'Heat trap': light-induced localized heating and thermionic electron emission from carbon nanotube arrays. *Solid State Commun.* **151,** 1105–1108 (2011).
42. Oida, S., Hannon, J. B., Tromp, R. M., McFeely, F. R. & Yurkas, J. A simple *in situ* method to detect graphene formation at SiC surfaces. *Appl. Phys. Lett.* **98,** 213106 (2011).
43. Malko, D., Neiss, C., Vines, F. & Gorling, A. Competition for graphene: graphynes with direction-dependent Dirac cones. *Phys. Rev. Lett.* **108,** 086804 (2012).
44. Vogt, P. *et al.* Silicene: compelling experimental evidence for graphenelike two-dimensional silicon. *Phys. Rev. Lett.* **108,** 155501 (2012).
45. Cahangirov, S., Topsakal, M., Akturk, E., Sahin, H. & Ciraci, S. Two- and one-dimensional honeycomb structures of silicon and germanium. *Phys. Rev. Lett.* **102,** 236804 (2009).
46. Tang, S. & Dresselhaus, M. S. Constructing anisotropic single-Dirac-cones in $Bi_{1-x}Sb_x$ thin films. *Nano Lett.* **12,** 2021–2026 (2012).

Acknowledgements

The authors acknowledge financial support from the Ministry of Science and Technology of China (MoST, grants 2012CB933401 and 2014CB643502), the National Natural Science Foundation of China (NSFC, grants 91433101, 21374050 and 51273093) and the Program for Changjiang Scholars and Innovative Research Team in University (PCSIRT, IRT1257). The authors thank Z. Li (Tsinghua University) for help with X-ray photoelectron spectroscope and X. Kong (Nankai University) and H. Li (Dalian Institute of Chemical Physics, Chinese Academy of Sciences) for mass spectrum measurements.

Author contributions

Y.C. conceived and directed the study. T.Z. and H.C. carried out most of the experiments and data analysis. Y.W. carried out some initial experiments. T.Z. and Y.C., together with H.C., prepared most of the manuscipt. H.C. synthesized most of the samples and prepared the movies. Y.W., P.X., N.Y. and Y.L. participated in some experiments, data analysis and discussions. K.Z., X.Y. and Z.L. participated in current measurements. All authors participated in project discussions and production of the final manuscript.

Additional information

Supplementary information is available in the online version of the paper. Reprints and permissions information is available online at www.nature.com/reprints. Correspondence and requests for materials should be addressed to Y.C.

Competing financial interests

A Chinese patent based on this work has been filed (application no. CN2014105392945).

Methods

The synthesis of the graphene sponge and preparation of the samples for experiments and characterization are provided in Supplementary Sections 'Materials synthesis' and 'Instruments and measurements conditions'. The graphene sponge samples in Fig. 2a,b were placed in a vertical vacuum tube (vacuum of 6.8×10^{-4} torr) to observe laser-induced propulsion. The laser spot areas for Fig. 2a,b were all ~4 mm^2. The diameter and height of the cylindrical sample were 10 and 11 mm, respectively, and the mass of the sample was ~0.86 mg. Two different graphene sponge samples were used in Fig. 2e and termed samples A and B. The samples in Fig. 2c,d,f were all sample A (as in Fig. 2e), and sample A had dimensions of $12 \times 7 \times 5$ mm^3 and a weight of 0.44 mg. Sample B in Fig. 2e had dimensions of $12.5 \times 8 \times 3.5$ mm^3 and a weight of 0.36 mg. The laser spot areas in Fig. 2c–f were all ~4.5 mm^2, and all the experiments were performed in a vacuum environment of 6.8×10^{-4} torr. The laser spot areas in Fig. 4 were all ~3.5 mm^2. In Fig. 4a, the distance between the sample and the metal container (acting as the current collection electrode) was ~2 mm and the vacuum was better than 5×10^{-6} torr. In Fig. 4d, the electron kinetic energy was measured using a concentric hemispherical electron energy analyser (CHA) on an XPS instrument with slight modification, and the graphene sponge was illuminated with a laser but without X-ray radiation. The vacuum of the XPS instrument was better than 6.7×10^{-9} torr. Measurement details are provided in Supplementary Section 'Instruments and measurements conditions'. In Fig. 4e, the laser wavelength was 450 nm and the power density was ~8.57×10^4 mW cm^{-2}. A digital oscilloscope with high enough sampling frequency was used to record the current signals in real-time.